JOURNAL OF MATERIALS SCIENCE 31 (1996) 3271–3280

Effect of physical and geometrical factors on interfacial debonding in the fibre push-out test: A new strength-based model

C. Y. YUE, N. L. LOH, L. L. LEE
School of Mechanical and Production Engineering, Nanyang Technological University, Nanyang Avenue, Singapore 2263

A strength-based model for the single-fibre push-out test has been developed. Using this model, the matrix stress, fibre stress and interfacial shear stress in a single fibre specimen subjected to push-out loading was considered. The effect of physical and geometrical factors on the stress distribution were evaluated in terms of the influence of relative moduli and sizes of the matrix and fibre, respectively. The propensity for debonding crack initiation at the interface arising from matrix yielding (due to normal stress) and interfacial yielding (due to shear stress) has been determined. The influence of these on the location of debonding crack initiation and the maximum debond force has also been studied.

1. Introduction

The properties of the fibre/matrix interface have a significant influence on the mechanical properties of composites. These interfacial properties include the interfacial shear (bond) strength, τ_i, interfacial frictional stress, τ_f, matrix shrinkage pressure on the fibre, P_0, interfacial coefficient of friction, μ, and the interfacial toughness, G_i. Recognition of the importance of interfacial properties has led to the development of a number of experimental techniques and theoretical models for assessing these properties. The commonly used tests are the push-out test, the micro-indentation test and the pull-out test, of which the single-fibre push-out test is most suitable for metal-matrix and ceramic-matrix composites.

Theoretical models on push-out have been developed on either a strength-based [1–3] or a fracture-based approach [4–6]. Although some of the analyses are rigorous and comprehensive [1, 4], they cannot be readily applied to experimental data to obtain the interfacial properties. On the other hand, other studies [7–9] are simplified and focused only on the effect of interfacial friction. In these cases, it was assumed that only frictional bonding exists at the interface, that is, there is no resistance to fibre slippage other than frictional bonding. The objective was to obtain the shear stress at the interface at which the fibre began to slide and this value was taken as an indication of the interfacial shear strength. This assumption is not valid for composite systems with chemical bonding at the interface whereby debonding takes place by the propagation of a mode II crack at the interface after crack initiation.

The complete stress field in the matrix and fibre and at the interface of an intact fibre has not been rigorously defined. Initially, the shear stress at the interface was assumed to be constant along the length of the fibre [10]. However, this assumption only provides a reasonable approximation if the embedded length of fibre is very short. Further studies [11] have shown that the interfacial shear stress is not constant along the embedded length but decays exponentially from the loaded end. Moreover, existing experimental work involves push-out tests of actual composites with fibres of less than 150 μm diameter. The small diameter fibres utilized did not allow experimental observation, and hence verification, of the failure processes predicted from the theoretical models adopted.

The aim of the present work was to present a comprehensive theoretical strength-based model which can be readily applied to push-out data to assess the interfacial properties. This model is an extension of a strength-based pull-out model [12] which has been found [13] to be useful and reliable. Next, the influence of the relative moduli ratio and specimen geometry on the stress distribution and point of crack initiation in the push-out specimen were investigated. Finally, the effect of Poisson's expansion of the fibre on the maximum push-out load and the debonding characteristics was examined. This is the first in a series of papers on the interfacial properties of metal-matrix and ceramic-matrix composites.

2. Development of the model

The set-up for the push-out test in the current model consists of a specimen (a single fibre embedded in a block of matrix or a thin slice cut from an as-fabricated composite) positioned over a hole in the centre of the support (see Fig. 1). It is assumed that the load is applied on to the fibre using a flat-faced indentor and the load–displacement curve is monitored.

0022–2461

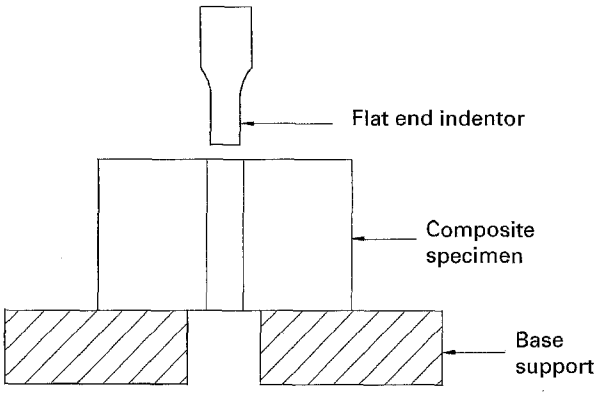

Figure 1 Schematic diagram of the push-out test.

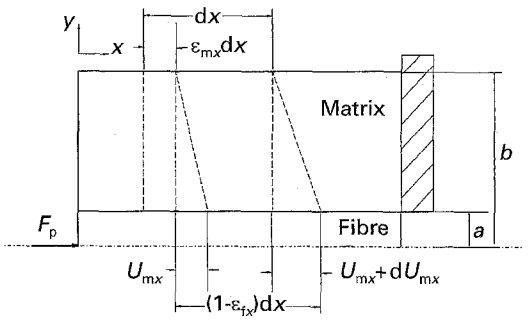

Figure 2 Elastic displacement of the fibre–matrix interface for the single-fibre push-out test.

The indentor is assumed to be much stiffer compared to the specimen so that it does not deform appreciably during loading.

A strength-based criterion for debonding crack initiation is assumed and the contribution of the frictional force to the debonding load during the debonding process is taken into account. The analysis developed for a single-fibre system in which the matrix and fibre are assumed to be linearly elastic up to failure is outlined below. The complete derivation of the model is presented in Appendices 1 and 2.

2.1. Stresses at the interface

When a load, F_p, is applied to a specimen, the specimen will deform elastically as shown in Fig. 2. The shear force on an elemental section, dx, at the interface is $2\pi a\tau_x dx$. This force is assumed to decrease linearly, in the y-direction, to zero at the circumferential surface of the matrix. From a consideration of the equilibrium of forces (see Appendix 1), the expressions for the compressive stress on the matrix, σ_{mx}, the axial stress on the fibre, σ_{fx}, and the interfacial shear stress, τ_x, can be shown to be

$$\sigma_{mx} = \frac{F_p}{\pi(b^2 - a^2)}\left[\psi + \frac{(1-\psi)\sinh(\alpha x) - \psi\sinh\alpha(L-x)}{\sinh(\alpha L)}\right] \quad (1)$$

$$\sigma_{fx} = \frac{F_p}{\pi a^2}\left[(1-\psi) + \frac{\psi\sinh\alpha(L-x) - (1-\psi)\sinh(\alpha L)}{\sinh(\alpha L)}\right] \quad (2)$$

$$\tau_x = \frac{F_p}{2\pi a}\left[\frac{\alpha(1-\psi)\cosh(\alpha x) + \alpha\psi\cosh\alpha(L-x)}{\sinh(\alpha L)}\right] \quad (3)$$

where

$$\alpha = \left\{2G_m \Big/ \left\{(b^2-a^2)\left[\left(\frac{b}{b-a}\right)\ln\left(\frac{b}{a}\right) - 1\right]\right\}\left[\frac{E_m(b^2-a^2) + E_f a^2}{E_f E_m a^2}\right]\right\}^{1/2} \quad (4)$$

$$\psi = \frac{E_m(b^2-a^2)}{E_f a^2 + E_m(b^2-a^2)} \quad (5)$$

x is the distance from the fibre-loaded end, b and a are the radii of the matrix and fibre, respectively, G_m and E_m are the shear and elastic modulus of the matrix, and E_f is the elastic modulus of the fibre. In these expressions, stresses with positive values are compressive while stresses with negative values are tensile in nature. The above equations can be utilized to assess the effect of physical and geometrical factors on the location where debonding is expected to be initiated in a push-out specimen. Information on the likely cause of debonding may also be established. Such analysis will be carried out in a latter section.

2.2. Push-out force for interfacial debonding

A strength-based model for the push-out test can now be developed on the basis of Equations 1, 2 and 3. In the push-out test, the load is usually applied at the exposed top surface of the fibre. It is generally believed and assumed that interfacial debonding initiates around the perimeter of the fibre face at which loading is applied. However, this assumption is not always valid. It will be demonstrated in Section 3.1 that, depending on the physical and geometrical factors, it is possible for the interface to debond at the perimeter of the fibre face at the opposite (unloaded) end. Therefore, it is important to examine whether the force for debonding crack initiation and the maximum push-out force are influenced by the position at which debonding occurs within the specimen. This will now be considered.

2.2.1. Debonding force

Expressions for the push-out force to initiate debonding can be developed for two cases: Case I for debonding crack initiation at the loaded (top) end, and Case II for debonding crack initiation at the unloaded (bottom) end of the fibre. Utilizing a strength-based

criterion, debonding initiates when the interfacial shear stress, τ_x, reaches the interfacial bond strength of the composite system, τ_i. The push-out force, F_i, required to initiate debonding can be obtained from Equation 3 by substituting τ_x with τ_i and rearranging to determine F_p (where $F_p = F_i$).

Case I. If the debonding crack initiates from the top face ($x = 0$), then the push-out force required to initiate debonding is given by

$$F_i = \frac{2\pi a\tau_i \sinh(\alpha L)}{\alpha(1-\psi) + \alpha\psi\cosh(\alpha L)} \quad (6)$$

Case II. If, on the other hand, the crack initiates from the opposite base end ($x = L$), then the corresponding push-out force required to initiate debonding is given by

$$F_i = \frac{2\pi a\tau_i \sinh(\alpha L)}{\alpha(1-\psi)\cosh(\alpha L) + \alpha\psi} \quad (7)$$

It is apparent that Equations 6 and 7 are different. This may lead to a significant and appreciable difference in the force for debonding crack initiation. This will be demonstrated clearly later for some practical fibre composite systems. The dependence of the push-out force to initiate debonding on the location from which debonding occurs is a factor which has not previously been recognized.

2.2.2. Maximum push-out force

Expressions for the maximum push-out force can also be developed for two cases: Case I for debonding crack initiation at the loaded (top) end, and Case II for debonding crack initiation at the unloaded (base) end of the fibre.

Case I, the case for debonding at $x = 0$. The criterion for debonding initiation is given by Equation 6. Once debonding occurs, the specimen compliance changes due to the formation of an interfacial crack and the maximum stress at the interface decreases to a value below τ_i. For further crack growth after crack initiation, the applied load has to be increased so that the shear stress which is a maximum at the crack front, τ_x, reaches the interfacial shear strength, τ_i.

When the crack has propagated along the length of the interface, a debonded region and a bonded region exist within the push-out specimen. The push-out force, F_p, required to ensure further crack propagation consists of (1) the force, F_{uy}, which is the force at the crack front when $\tau_x = \tau_i$, to allow further debonding of the remaining bonded length, l_u, of the fibre, and (2) the force, F_f, to overcome frictional push-out due to the shrinkage pressure of the matrix on to the debonded length, l_d, of the fibre.

The force, F_{uy}, is obtained by substituting L with l_u in Equation 6

$$F_{uy} = \frac{2\pi a\tau_i \sinh(\alpha l_u)}{\alpha(1-\psi) + \alpha\psi\cosh(\alpha l_u)} \quad (8)$$

The debonded area is $2\pi a$ and the interfacial frictional shear stress is τ_f (where $\tau_f = \mu P_0$ and μ is the interfacial coefficient of friction, P_0 is the residual shrinkage pressure in the matrix. P_0 arises due to processing and mismatch in thermal properties between the fibre and matrix). The frictional push-out force, F_f, for the debonded section, l_d, is thus given by

$$F_f = 2\pi a\tau_f(L - l_u) \quad (9)$$

The total push-out force, F_p, is the sum of shear force, F_{uy}, in the bonded region and frictional force, F_f, in the debonded region such that

$$F_p = \frac{2\pi a\tau_i \sinh\alpha(L - l_d)}{\alpha(1-\psi) + \alpha\psi\cosh\alpha(L - l_d)} + 2\pi a\tau_f l_d \quad (10)$$

Equation 10 describes the force necessary for steady progressive debonding at the interface. The changes in the total push-out force, F_p, frictional push-out force, F_f, and the debonding force, F_{uy}, with the position of the crack front for a copper fibre–epoxy system are as shown in Fig. 3. In the analysis, the following values were assumed: $E_m = 4$ GPa, $E_f = 120$ GPa, $\nu_m = 0.3$, $\nu_f = 0.35$, $b = 20.5$ mm, $a = 1.5$ mm, $\tau_i = 10$ MPa, $\mu = 0.25$ and $P_0 = 20$ MPa.

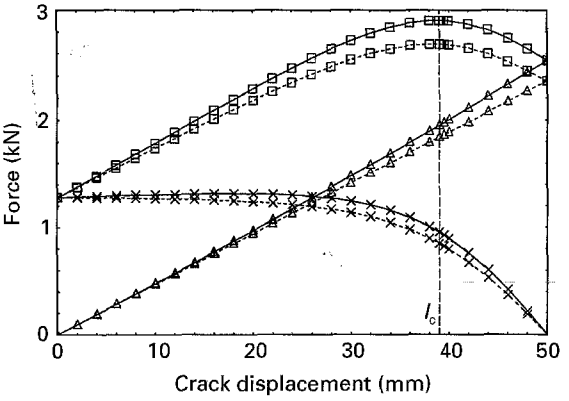

Figure 3 Variation of (□) total push-out force, F_p, (△) frictional force, F_f, and (x) debonding force, F_{uv}, during the debonding process: (——) with and (– – –) without Poisson's expansion.

It can be seen in Fig. 3 that F_f varies linearly with the position of the crack front. In contrast, the debonding force, F_{uy}, is constant initially over a short range but decreases progressively as the area which remains bonded in the specimen diminishes with advancing crack front. Because F_{uy} is the force required to ensure that τ_x is equal to τ_i, the results indicate that beyond a certain residual bonded length, the force required to maintain the stress at the edge of the crack at τ_i falls rapidly. This gives rise to a peak value, $F_{p(max)}$, in the total push-out force, F_p (see Fig. 3). It is apparent from Fig. 3 that catastrophic interfacial failure occurs once $F_{p(max)}$ is reached, because the push-out force required for the final stages of debonding is less than $F_{p(max)}$. This indicates that there exists a critical length of the bonded region, l_c, which denotes the transition of the debonding crack propagation from a steady to a catastrophic behaviour.

Therefore, progressive debonding would occur in specimens with an embedded length $L > l_c$. The push-out force, F_d, for complete debonding for such

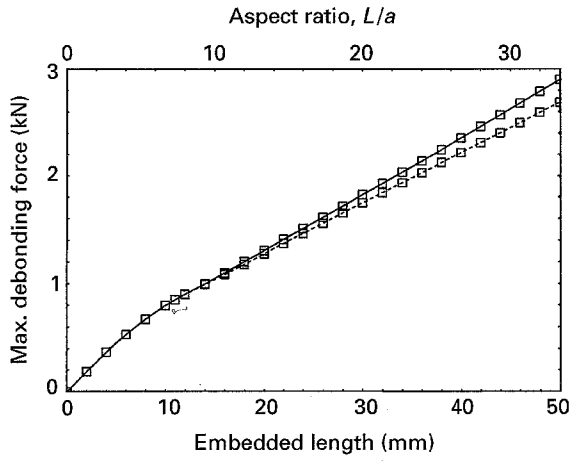

Figure 4 Effect of Poisson's expansion of fibre on maximum debonding force, $F_{p(max)}$ (——) with and (– – –) without Poisson's expansion.

specimens corresponds to the maximum value of F_p at $L - l_d = l_c$.

$$F_d = \frac{2\pi a\tau_i \sinh(\alpha l_c)}{\alpha(1-\psi) + \alpha\psi\cosh(\alpha l_c)} + 2\pi a\tau_f(L - l_c) \quad (11)$$

However, catastrophic failure occurs in specimens with $L < l_c$. The push-out force for complete debonding, F_d, in this case is the same as the force for debonding crack initiation, F_i, given by Equation 6. It is important to note that the maximum load recorded in an experimental push-out test is the push-out force for complete debonding, F_d.

The variation of F_d with fibre embedded length, L, for the copper fibre–epoxy system is as shown in Fig. 4. It can be seen in Fig. 4 that the plot is non-linear in the region $L < l_c$ but is linear for the region $L > l_c$.

Case II, the case for debonding at $x = L$. A similar analysis can be made for the specimens in which debonding initiates from the base end. The total push-out force is now given by

$$F_p = \frac{2\pi a\tau_i \sinh\alpha(L - l_d)}{\alpha\psi + \alpha(1-\psi)\cosh\alpha(L - l_d)} + 2\pi a\tau_f l_d \quad (12)$$

For specimens with embedded length $L \ll l_c$, the push-out force for complete debonding, F_d, is equal to F_i in Equation 7. For specimens with $L \gg l_c$, F_d is given by

$$F_d = \frac{2\pi a\tau_i \sinh(\alpha l_c)}{\alpha\psi + \alpha(1-\psi)\cosh(\alpha l_c)} + 2\pi a\tau_f(L - l_c) \quad (13)$$

The effect on F_d of the location at which crack initiation occurs will be considered later.

2.3. Effect of Poisson's expansion

The fibre undergoes some radial expansion under the action of the push-out load. This radial expansion in the fibre (due to the Poisson ratio effect) has a significant influence on the push-out load in the case of a fibre with large aspect ratio or lower stiffness. The radial expansion induces an additional compressive force from the matrix to act on the fibre. This is in addition to compressive stresses on the fibre which develop during processing due to shrinkage of the matrix on to the fibre. Therefore, the frictional force at the interface will increase. It can be shown (Appendix 2) that the push-out force, F_p, is given by

$$F_p = F_{uy}\exp\left(\frac{2\mu k}{a} l_d\right) + \frac{\pi a^2 P_0}{k}\left[\exp\left(\frac{2\mu k}{a} l_d\right) - 1\right] \quad (14)$$

where $k = E_m v_f/E_f(1 + v_m)$ and v_m and v_f are the Poisson's ratios of the matrix and fibre, respectively.

The effect of Poisson's expansion on the variation of F_p, F_{uy} and F_f with advancing crack front, l_d, is illustrated in Fig. 3. It can be seen that when Poisson's expansion of the fibre is taken into account, F_{uy} has the same trend but a higher magnitude than when the effects are ignored. This is due to the higher radial fibre stress which hinders debonding. The frictional force, F_f, increases exponentially with the debonded length when Poisson's expansion effect is taken into account (see Fig. 3). In contrast, F_f increases linearly with the debonded fibre length if the effect is ignored. Thus, Poisson's expansion leads to a higher frictional force. The total push-out force, F_p, is higher for the case with Poisson's expansion. For the copper–epoxy system considered, Poisson's expansion effects did not seem to affect l_c significantly.

The effect of Poisson's expansion on the plot of maximum debonding load, F_d, against embedded length, L, for the copper fibre–epoxy system is as shown in Fig. 4. It can be seen in Fig. 4 that at $L > l_c$, the push-out load without Poisson's effect increases linearly with L whereas that with Poisson's effect increases exponentially. This effect is more pronounced for specimens with higher embedded length or larger aspect ratio. In some systems such as the copper fibre–epoxy system considered, a linear approximation may be assumed for the exponential increase.

3. Results and discussion

Using the above theoretical model, the effect of the relative moduli ratio ($R = E_m/E_f$) and the specimen geometry ($Q = b/a$) of a composite system on the stress distributions will now be studied. Of interest is the influence of these two factors on the point of crack initiation in a push-out specimen. The influence of the point of debonding initiation on the characteristics of the push-out force and the critical embedded length, l_c, will also be considered.

3.1. Effect of modulus ratio, $R = E_m/E_f$, on the stress distribution

The effect of the modulus ratio, R, on the interfacial shear stress distribution and the compressive axial stress in the fibre and matrix will now be considered. For the plots shown in Figs 5–9, the fibre modulus was fixed at 400 GPa while the matrix modulus was varied

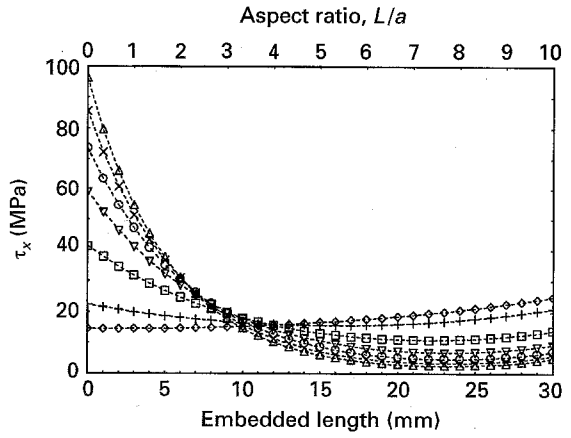

Figure 5 Variation of interfacial shear stress, τ_x, with $R = E_m/E_f$: (◇) 0.001, (+) 0.025, (□) 0.1, (▽) 0.2, (○) 0.3, (×) 0.4, (△) 0.5.

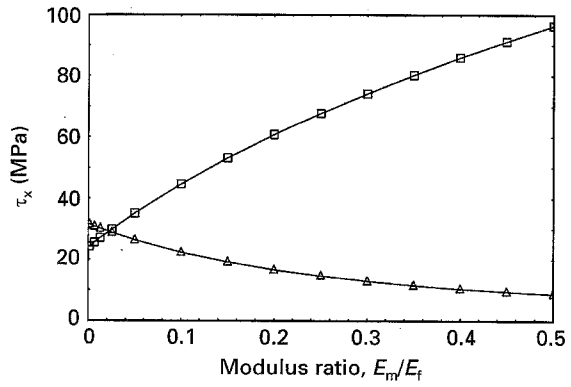

Figure 6 Variation of interfacial shear stress, τ_x, at the top, $x = 0$ (□), and the base, $x = L$(△).

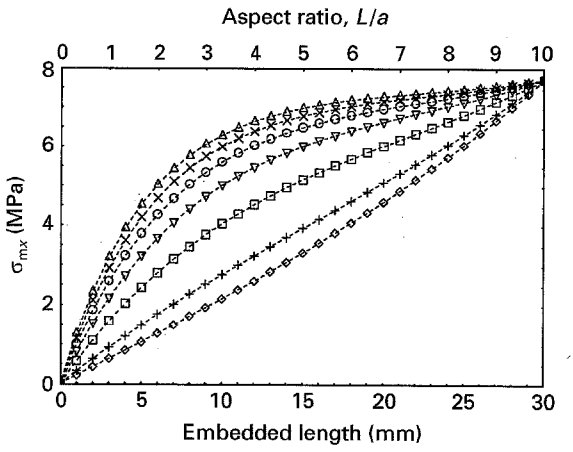

Figure 7 Variation of longitudinal matrix stress, σ_{mx}, along the embedded length. For key, see Fig. 5.

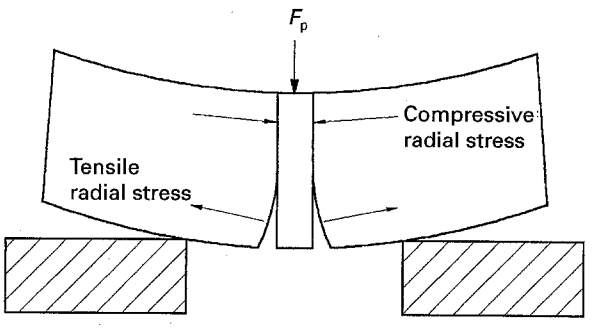

Figure 8 Effect of mode I crack propagation on interfacial debonding.

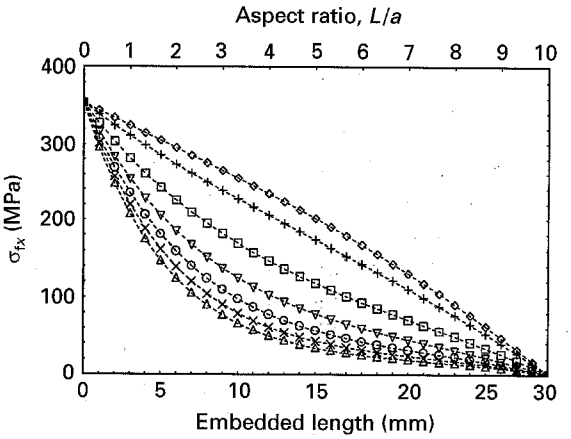

Figure 9 Variation of axial fibre stress, σ_{fx}, along the embedded length with R. For key, see Fig. 5.

to obtain different values of R. The matrix and fibre radius were fixed at 20.5 and 3 mm, respectively (fixed geometry ratio of 41/6) and a push-out load of 10 kN was assumed for an embedded length of 30 mm.

The values of R considered in this analysis cover a wide range of moduli ratio for polymer-matrix (PMC), metal-matrix (MMC) and ceramic-matrix composites (CMC). Typical values of R for PMCs are 0–0.1 (0.067 for glass–epoxy), values of R for MMCs are 0.1–0.4 (0.325 for SiC–Ti) and for CMCs are 0.1–0.8 (0.29 for SiC–RBSN).

3.1.1. Effect of modulus ratio on interfacial debonding

Interfacial debonding will initiate at the position where the interfacial shear stress is maximum. From the plots of τ_x versus embedded length in Fig. 5, it can be seen that for most values of R at a fixed geometry ratio of 41/6, the top-end or loaded-end of the specimen experiences high shear stress concentrations. The shear stresses decrease rapidly along the embedded length away from the loaded end. It is apparent from Fig. 5 that in cases where $R > 0.025$, the debond crack will initiate from the loaded end ($x = 0$). This implies that interfacial debonding in push-out specimens in which the fibre is surrounded by an appreciable amount of matrix (geometry ratio of 41/6) in MMCs and CMCs (where $R > 0.025$) initiate at the top loaded end of the fibre. This assumption is only correctly made in some existing published work on push-out tests in MMCs and CMCs.

On the other hand, the shear stress distribution becomes more uniform along the embedded length when R approaches 0.025. In this case, the shear stresses at both ends are similar and simultaneous debonding may be expected to take place. For $R < 0.025$, the shear stress distribution is reversed. The shear stress at the base is higher than at the loaded end and debonding will initate at the bottom and propagate upwards. The above R values fall within the range of that for PMCs. Hence, the above analysis indicates that the assumption of interfacial debonding initiation from the top loaded end is clearly erroneous for certain PMCs. The point of debonding

initiation has to be established for individual PMCs to avoid misleading evaluation of push-out data.

A clearer representation of the shear stresses at the top ($x = 0$) and base ($x = L = 30$ mm) is shown in Fig. 6. The shear stress at the top increases with R, whereas that at the base decreases with R. This analysis clearly contradicts the assumption made in many studies [1, 4, 6] that the debonding crack always initiates from the loaded end for the same push-out configuration. Whenever possible, this initiation point should be determined physically during the test or from shear stress analysis as this will affect the interpretation of results obtained, as will be discussed in Section 3.4. Similar plots can be generated to determine the influence of R on the point of interfacial crack initiation for any fixed value of geometry ratio.

3.1.2. Effect on matrix yielding

The stress distribution in the matrix, σ_{mx}, is shown in Fig. 7. It can be seen that σ_{mx} is compressive over the whole embedded length for all values of R. The stress is 0 at the free surface ($x = 0$) and increases to a maximum at the base ($x = L$).

The strength of a fibre-reinforced composite is greatly improved over that of the monolithic matrix material due to the load-bearing ability of the fibres. Thus, to obtain a high-strength composite, the load transfer from the matrix to the fibre must be effective. From Fig. 7, it is observed that the stress transfer from the matrix to the fibre becomes less effective as R increases. In other words, the stress transfer in composite systems with high R is ineffective.

Matrix yielding is another important factor to be considered. Failure initiation by matrix yielding may occur in composite systems where $\tau_i > \sigma_{mx(yield)}$. This may result from a strong interface or interphase and/or a large compressive force of the matrix on the fibre due to the difference in the thermal coefficients of expansion. For all values of R, σ_{mx} is maximum at the base. Therefore, failure by matrix yielding will only occur at the base for all PMCs, MMCs and CMCs. Debonding from the base will further be favoured if large bending stresses exists due to a large support hole size or testing of very thin specimens (see Fig. 8). In this case, matrix yielding will be coupled with mode I crack propagation.

3.1.3. Effect on fibre failure

The variation of axial stress distribution along the fibre with R is as shown in Fig. 9. The axial stress is compressive along the fibre length, being maximum at the loaded end and decreasing to 0 at the base. The high stress concentration at the top of the fibre can lead to fibre failure (especially if the fibres are brittle), thereby rendering the push-out test void.

Initially, sharp-edged indentors, similar to the pyramid indentors used in the microhardness test, were used for micro-indentation or push-in test [10, 14, 15]. The extremely high stress concentrations at the fibre surface in contact with the sharp edge will give rise to rupture or splitting of brittle fibre. Desaeger and Verpoest [14] reported that some of the glass fibres ruptured but all the carbon fibres split during the indentation tests. The phenomenon of carbon fibre splitting is a result of the inherent microstructure of carbon. The validity of the results obtained from the push-in or push-out of such materials is thus questionable.

The sharp-edged indentor was consequently replaced by a flat-end indentor. However, the fibre may still fail before debonding if the composite system has a high interfacial shear strength. This has been observed in the push-out of glass rod (diameter 5 mm) from an epoxy matrix using a flat-end indentor [16]. In contrast, the pull-out test of glass fibres has been carried out successfully on the same composite system [17]. The solution to this may be to restrict the push-out test of such systems to thin specimens. Therefore, it is important to realize that the push-out test (or any other test) may not be suitable for assessing the interfacial properties of all materials.

3.2. Effect of specimen geometry

The effect of specimen geometry (b/a ratio) on the point of debonding initiation was studied for a steel fibre–epoxy matrix system ($R = 0.02$), a silicon carbide fibre–aluminium matrix system ($R = 0.175$) and a silicon carbide fibre–zirconia matrix ($R = 0.29$) system. The parameters used in the analysis are given in Table I. The radius of the fibre, a, was fixed at 3 mm while the radius of the matrix, b, was varied to obtain different b/a ratios. A push-out force of 10 kN was also assumed for a fibre embedded length of 30 mm.

The variation of the interfacial shear stress levels at the top ($x = 0$) and at the base ($x = L$) of the specimen with specimen geometry is illustrated in Fig. 10a–c. The difference in stresses at the top and the base of the specimen approaches a constant value as b/a increases. This difference is highest for the SiC–zirconia system and lowest for the steel–epoxy system.

It can be seen in Fig. 10 that a top–base failure transition occurs in the PMC, MMC and CMC systems considered. This transition point occurs at a higher b/a ratio for the steel–epoxy PMC system ($b/a = 7$) than for the SiC–Al MMC system ($b/a = 3$) and the SiC–zirconia CMC system ($b/a = 2$). Thus, the point of debonding initiation in all composite systems is dependent on the specimen geometry ratio. This has serious implications on the selection of test fibres in a push-out test.

Usually, a composite (containing many embedded fibres which are assumed to be in parallel) which is sliced in a direction perpendicular to the fibre axis is utilized in a push-out test. The b/a ratio of individual fibres in such a composite slice may be taken to be half

TABLE I Parameters of the composite systems

System	E_m (GPa)	E_f (GPa)	ν_m	ν_f
Steel–epoxy	4	200	0.3	0.3
Silicon carbide–aluminium	70	400	0.33	0.3
Silicon carbide–zirconia	200	400	0.3	0.3

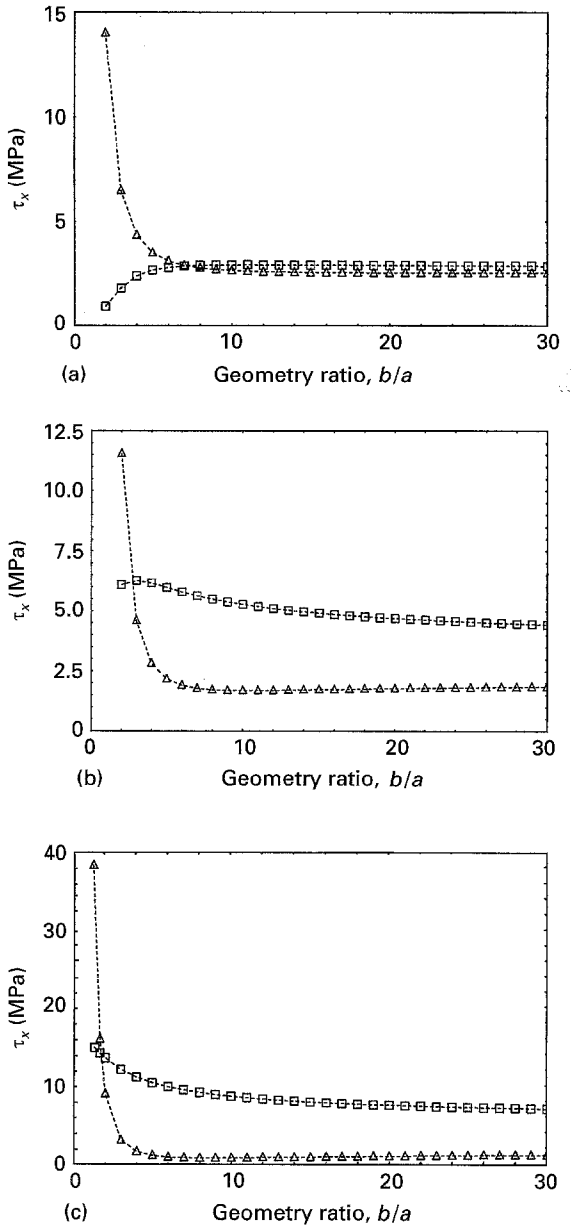

Figure 10 Effect of geometry ratio b/a on interfacial shear stress, τ_x, at the (□) top and (△) base for (a) steel–epoxy system, (b) silicon carbide–aluminium system and (c) silicon carbide–zirconia system.

the distance between the centres of two neighbouring fibres. It is apparent from Fig. 10 that the point of debonding initiation for all fibres in such a specimen would not be the same. Debonding initiation in test-fibres within a fibre bundle (small b/a ratio) will occur at the unloaded (base) end of the fibres whilst that in test-fibres away from fibre bundles will occur at the loaded (top) end. Errors will be introduced if data from fibres under both situations are evaluated together.

3.3. Influence of point of crack initiation

It has been established in an earlier section that the interfacial crack may initiate either at the loaded end or the base of the system. The influence of the point of crack initiation on the crack initiation force and the debonding force will now be considered. The pertinent equations for debonding initiation from the loaded

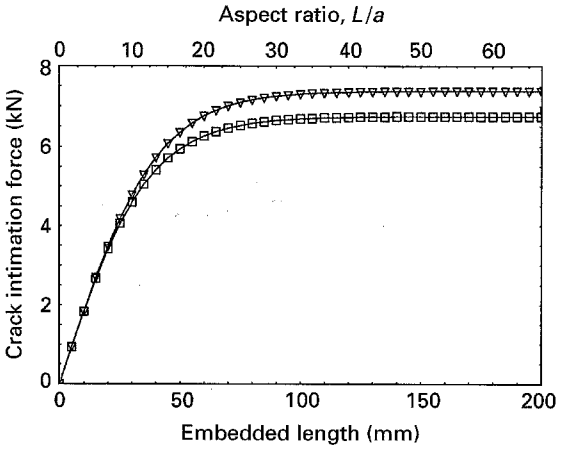

Figure 11 Effect of crack initiation point on crack initiation force, F_i: crack initiates at $x = 0$ (▽) and at $x = L$ (□).

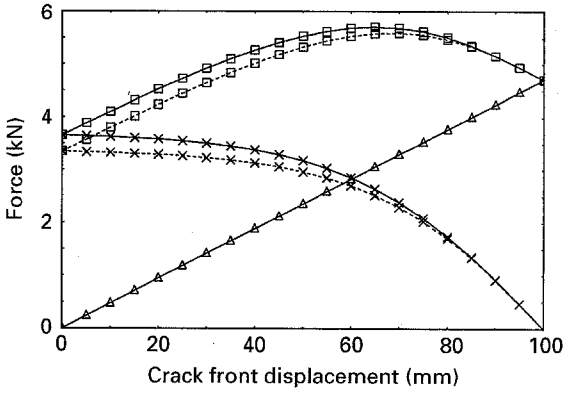

Figure 12 Effect of crack initiation point on total push-out force, F_p, and debonding force, F_{uv}: crack initiation at (——) $x = 0$ and (– – –) $x = L$. For key, see Fig. 3.

(top) end are given by Equations 6 and 11 while that for the unloaded (base) end are given by Equations 7 and 12. The steel–epoxy system considered in Section 3.2 with a geometry ratio of 41/6 will be used for the analysis in this section. For this system, the crack propagation has been predicted to initiate from the base.

The effect of crack initiation at $x = 0$ and $x = L$ on the crack initiation force, F_i, is shown in Fig. 11. For both cases, F_i increases rapidly with embedded length initially before it plateaus off to a constant value for large embedded length. However, the force for debonding initiation at the top is higher than that at the base (which force is higher is actually dependent on the system's parameters, α and ψ). The values of both forces are close to each other for small embedded length but the difference becomes significant for large embedded length. Because, for this system, the crack has been predicted to propagate from the base, the assumption of crack propagation from the top will give an overestimation of the crack initiation force, F_i.

The effect of debonding initiation point on the debonding force, F_p, and the maximum debonding force, $F_{p(max)}$, is shown in Fig. 12. Debonding initiation from the loaded end results in a higher compressive force, F_{uy}, at the crack-tip to ensure further crack propagation. This, consequently, gives rise to a larger maximum debonding force. Similarly, an assumption of

crack propagation from the top will lead to an overestimation of $F_{p(max)}$.

4. Conclusion

The stress distributions for τ_x, σ_{mx} and σ_{fx} along the embedded length of an intact fibre are affected by R, the moduli ratio, and b/a, the geometry ratio of the matrix and fibre, of the push-out specimen. The force for initiation of interfacial debonding, F_i, and the total debonding force, $F_d = F_{p(max)}$, is dependent on the point of debonding crack initiation. A top–base debonding initiation transition occurs in PMCs, MMCs and CMCs and this is dependent on both R and b/a. Debonding initiation arising from matrix failure will occur more readily at the base of the specimen. Fibre failure tends to occur at the loaded end. The effect of Poisson's expansion of a fibre is to increase the maximum push-out load.

Appendix 1. Stress distributions

Consider an elemental section, dx, of the matrix and fibre as shown in Fig. 2. From geometrical considerations

$$(1 - \varepsilon_{fx})dx - (U_{mx} + dU_{mx}) + U_{mx} + \varepsilon_{mx}dx = dx \tag{A1}$$

Simplifying

$$\frac{dU_{mx}}{dx} = \varepsilon_{mx} - \varepsilon_{fx} \tag{A2}$$

Consider the stresses acting on an element of the fibre and of the matrix at the interface of the push-out specimen illustrated in Fig. A1. From the equilibrium of forces on the matrix element

$$\tau_x = \frac{(b^2 - a^2)}{2a}\frac{d\sigma_{mx}}{dx} \tag{A3}$$

For the fibre element

$$\tau_x = -\frac{a}{2}\frac{d\sigma_{fx}}{dx} \tag{A4}$$

Taking the cross-section at any distance x, the push-out force can be written as

$$F_p = \pi a^2 \sigma_{fx} + \pi(b^2 - a^2)\sigma_{mx} \tag{A5}$$

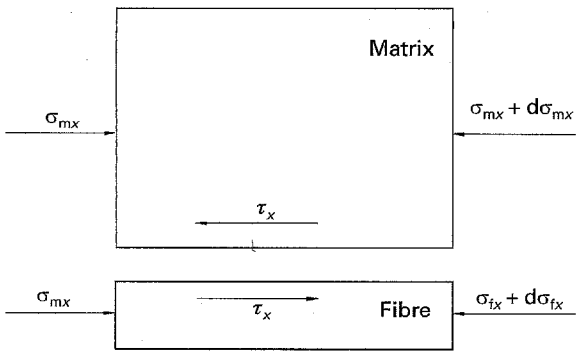

Figure A1 Stresses acting on an element of fibre and matrix.

The displacement of the matrix in the x-direction, U_{mx}, can be written as

$$U_{mx} = \int_a^b \frac{\tau_{x,y}}{G_m} dy \tag{A6}$$

where $\tau_{x,y}$ is the shear stress acting on the matrix in the x-direction at a distance y from the centre of the fibre–matrix system.

The shear stress is zero at the circumferential surface. The shear force is assumed to decrease linearly in the y-direction from S_i at the interface to 0 at the circumferential surface of the matrix. The shear force at the interface ($r = a$) is given by

$$S_i = 2\pi a \tau_x dx \tag{A7}$$

and the shear force at a distance y is given by

$$\tau_{x,y} = \tau_x \frac{a}{y}\left(\frac{b - y}{b - a}\right) \tag{A8}$$

Substituting Equation A8 into Equation A7 gives

$$U_{mx} = \int_a^b \frac{\tau_x}{G_m}\frac{a}{y}\left(\frac{b - y}{b - a}\right)dy$$

$$= \frac{\tau_x a}{G_m}\left[\frac{b}{(b - a)}\ln\left(\frac{b}{a}\right) - 1\right] \tag{A9}$$

Differentiating Equations A3 and A9 with respect to x

$$\frac{d\tau_x}{dx} = \left(\frac{b^2 - a^2}{2a}\right)\frac{d^2\sigma_{mx}}{dx^2} \tag{A10}$$

$$\frac{dU_{mx}}{dx} = \frac{a}{G_m}\left[\frac{b}{(b - a)}\ln\left(\frac{b}{a}\right) - 1\right]\frac{d\tau_x}{dx} \tag{A11}$$

Substituting Equation A10 into Equation A11 gives

$$\frac{dU_{mx}}{dx} = \frac{a}{G_m}\left[\frac{b}{(b - a)}\ln\left(\frac{b}{a}\right) - 1\right]\left(\frac{b^2 - a^2}{2a}\right)\frac{d^2\sigma_{mx}}{dx^2} \tag{A12}$$

Equation A2 can be expressed in terms of the theory of elasticity

$$\frac{dU_{mx}}{dx} = \frac{\sigma_{mx}}{E_m} - \frac{\sigma_{fx}}{E_f} \tag{A13}$$

Substituting Equation A13 into Equation A12 results in

$$\frac{d^2\sigma_{mx}}{dx^2} = 2G_m\left\{(b^2 - a^2)\left[\frac{b}{(b - a)}\ln\left(\frac{b}{a}\right) - 1\right]\right\}^{-1} \times\left(\frac{\sigma_{mx}}{E_m} - \frac{\sigma_{fx}}{E_f}\right) \tag{A14}$$

Rearranging Equation A5

$$\sigma_{fx} = \frac{F_p}{\pi a^2} - \frac{\pi(b^2 - a^2)}{\pi a^2}\sigma_{mx}$$

$$= \frac{1}{a^2}\left[\frac{F_p}{\pi} - (b^2 - a^2)\sigma_{mx}\right] \tag{A15}$$

Substituting Equation A15 into Equation A14 gives

$$\frac{d^2\sigma_{mx}}{dx^2} = 2G_m\left\{(b^2-a^2)\left[\frac{b}{(b-a)}\ln\left(\frac{b}{a}\right)-1\right]\right\}^{-1}\left\{\frac{\sigma_{mx}}{E_m}-\frac{1}{a^2E_f}\left[\frac{F_p}{\pi}-(b^2-a^2)\sigma_{mx}\right]\right\}$$

$$= 2G_m\left\{(b^2-a^2)\left[\frac{b}{(b-a)}\ln\left(\frac{b}{a}\right)-1\right]\right\}^{-1}\left\{\frac{1}{E_m}+\frac{(b^2-a^2)}{E_fa^2}\right\}\sigma_{mx}$$

$$-2G_mF_p\left\{\pi a^2E_f(b^2-a^2)\left[\frac{b}{(b-a)}\ln\left(\frac{b}{a}\right)-1\right]\right\}^{-1} \quad \text{(A16)}$$

Equation A16 is of the form

$$\frac{d^2\sigma_{mx}}{dx^2} = A\sigma_{mx} + B \quad \text{(A17)}$$

where

$$A = 2G_m\left\{(b^2-a^2)\left[\frac{b}{(b-a)}\ln\left(\frac{b}{a}\right)-1\right]\right\}^{-1} \times\left\{\frac{E_fa^2+E_m(b^2-a^2)}{E_mE_fa^2}\right\}$$

$$B = -2G_mF_p\left\{\pi a^2E_f(b^2-a^2)\left[\frac{b}{(b-a)}\ln\left(\frac{b}{a}\right)-1\right]\right\}^{-1}$$

The solution to Equation A17 is

$$\sigma_{mx} = \frac{F_p}{\pi(b^2-a^2)} \times\left[\psi+\frac{(1-\psi)\sinh(\alpha x)-\psi\sinh\alpha(L-x)}{\sinh(\alpha L)}\right] \quad \text{(A18)}$$

To obtain σ_{fx}, substitute Equation A18 into Equation A14

$$\sigma_{fx} = \frac{F_p}{\pi a^2}\left[(1-\psi)+\frac{(\psi-1)\sinh(\alpha x)+\psi\sinh\alpha(L-x)}{\sinh(\alpha L)}\right] \quad \text{(A19)}$$

Differentiating Equation A19 with respect to x

$$\frac{d\sigma_{fx}}{dx} = \frac{F_p}{\pi a^2}\left[\frac{\alpha(\psi-1)\cosh(\alpha x)-\alpha\psi\cosh\alpha(L-x)}{\sinh(\alpha L)}\right] \quad \text{(A20)}$$

Finally, substitute Equation A20 into Equation A4 to obtain the expression for τ_x

$$\tau_x = \frac{F_p}{2\pi a}\left[\frac{\alpha(1-\psi)\cosh(\alpha x)+\alpha\psi\cosh\alpha(L-x)}{\sinh(\alpha L)}\right] \quad \text{(A21)}$$

Appendix 2
Push-out against friction

When the fibre/matrix interface has debonded, the force against the push-out of the fibre is the frictional force at the interface. This frictional force is governed by the matrix shrinkage pressure, P_0, the interfacial frictional coefficient, μ, and the Poisson's expansion of the fibre due to the compressive axial force.

The single fibre push-out model is illustrated in Fig. A2. Consider the forces acting on the fibre element, dl,

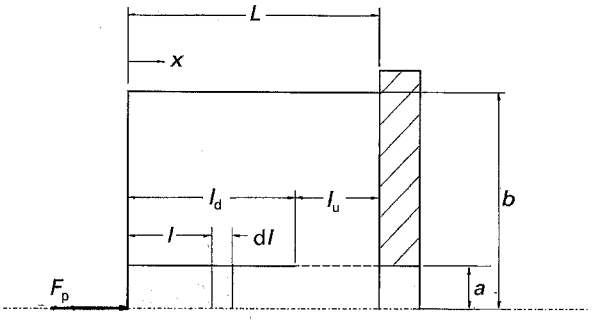

Figure A2 Partial debonding and partial frictional sliding of a single-fibre specimen.

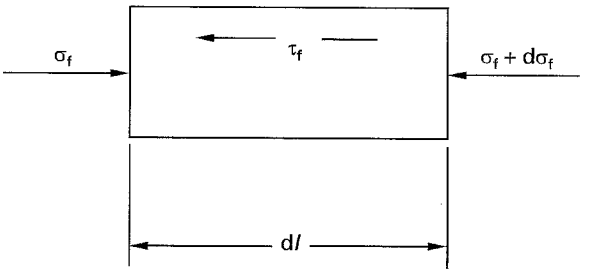

Figure A3 Stresses on an elemental length, dl, of the debonded region.

in Fig. A3. From the equilibrium of forces on the fibre element, dl, we have

$$\pi a^2 d\sigma_f = -2\pi a\tau_f dl \quad \text{(A22)}$$

such that

$$\frac{d\sigma_f}{dl} = -\frac{2\tau_f}{a} \quad \text{(A23)}$$

where σ_f is the compressive stress on the fibre and τ_f is the frictional stress at the interface. The value of τ_f is related to the matrix shrinkage pressure and the interfacial frictional coefficient by $\tau_f = \mu P_0$. Substituting this into Equation A23 gives

$$\frac{d\sigma_f}{dl} = -\frac{2\mu P_0}{a} \quad \text{(A24)}$$

The frictional force over the debonded region can be obtained by integrating Equation A24 over the debonded region. Because P_0 can be considered a constant for a rigid fibre and μ is a constant, we have

$$F_f = 2\pi a\mu P_0 l_d \quad \text{(A25)}$$

Effect of Poisson's expansion of the fibre

For a fibre of lower stiffness or high aspect ratio, the effect of Poisson's expansion is significant due to the compressive axial force. The Poisson's expansion of the fibre increases the effective matrix shrinkage pressure on the fibre and thus increases the interfacial friction. Because the axial compressive stress, σ_f, of the fibre varies along the embedded length, the radial expansion strain of the fibre is related to σ_f by

$$\varepsilon_r = \frac{\nu\sigma_f}{E} \tag{A26}$$

The thick-walled cylinder theory can be applied to determine the increase in shrinkage pressure due to Poisson's expansion. Substituting the expression for radial expansion strain into the thick-walled cylinder theory results in a pressure increment of

$$P_i = \frac{E_m \nu_f \sigma_f}{E_f(1 + \nu_m)} \tag{A27}$$

The frictional stress at the interface is given by

$$\begin{aligned}\tau_f &= \mu\left[P_0 + \frac{E_m\nu_f\sigma_f}{E_f(1+\nu_m)}\right] \\ &= \mu(P_0 + k\sigma_f)\end{aligned} \tag{A28}$$

where $k = E_m\nu_f/E_f(1 + \nu_m)$.

Substituting Equation A28 into Equation A23 and rearranging

$$\frac{d\sigma_f}{dl} + \frac{2\mu k\sigma_f}{a} = -\frac{2\mu P_0}{a} \tag{A29}$$

This is a first-order differential equation with solution given by

$$\exp\left(\frac{2\mu k}{a}l\right)\sigma_f = -\frac{P_0}{R}\exp\left(\frac{2\mu k}{a}l\right) + C \tag{A30}$$

The constant C can be evaluated from the boundary condition $\sigma_f = 0$ at $l = L - l_u = l_d$. The push-out force on the fibre due to friction over a debonded region, l_d, is given by

$$F_f = \frac{\pi a^2 P_0}{R}\left[\exp\left(\frac{2\mu R}{a}l_d\right) - 1\right] \tag{A31}$$

Effect of friction in the debonding process

When the crack has propagated partially along the length of the interface, two distinct regions exist: the debonded region and the bonded region. The compressive force, F_x, acting on the fibre at $0 \leqslant x \leqslant l_d$ can be obtained by multiplying Equation A30 by the cross-sectional area of the fibre such that

$$F_x\exp\left(\frac{2\mu k}{a}x\right) = -\frac{\pi a^2 P_0}{k}\exp\left(\frac{2\mu k}{a}x\right) + D \tag{A32}$$

The constant, D, can be evaluated from the boundary condition $F_x = F_{uy}$ at $x = l_d$.

$$D = \left[F_{uy} + \frac{\pi a^2 P_0}{k}\right]\exp\left(\frac{2\mu k}{a}l_d\right) \tag{A33}$$

The push-out force is given by the value of F_x at $x = 0$

$$F_p = F_{uy}\exp\left(\frac{2\mu k}{a}l_d\right) + \frac{\pi a^2 P_0}{k}\left[\exp\left(\frac{2\mu k}{a}l_d\right) - 1\right] \tag{A34}$$

References

1. C. H. HSUEH, *Acta Metall. Mater.* **38** (1990) 403.
2. D. K. SHETTY, *J. Am. Ceram. Soc.* **71** (1988) C107.
3. J. D. BRIGHT, D. K. SHETTY, C. W. GRIFFIN and S. LIMAYE, *ibid.* **72** (1989) 1891.
4. C. LIANG and J. W. HUTCHINSON, *Mech. Mater.* **14** (1993) 207.
5. R. J. KERANS and T. A. PARTHASARATHY, *J. Am. Ceram. Soc.* **74** (1991) 1585.
6. R. N. SINGH and M. SUTCU, *J. Mater. Sci.* **26** (1991) 2547.
7. C. J. YANG, S. M. JENG and J. M. YANG, *Scritpa Metall. Mater.* **24** (1990) 469.
8. J. D. BRIGHT, S. DANCHAIVIJIT and D. K. SHETTY, *J. Am. Ceram. Soc.* **74** (1991) 115.
9. D. B. MARSHALL, *ibid.* **67** (1984) C259.
10. D. B. MARSHALL and W. C. OLIVER, *ibid.* **70** (1987) 542.
11. M. C. WATSON and T. W. CLYNE, *Acta Metall. Mater.* **40** (1992) 131.
12. C. Y. YUE and W. L. CHEUNG, *J. Mater. Sci.* **27** (1992) 3173.
13. *Idem, ibid.* **27** (1992) 3183.
14. M. DESAEGER and I. VERPOEST, *Compos. Sci. Technol.* **48** (1993) 215.
15. J. F. MANDELL, J. H. CHEN and F. J. McGARRY, *Int. J. Adhes. Adhes.* **1** (1980) 40.
16. C. Y. YUE and L. L. LEE, unpublished work (1994).
17. C. Y. YUE and H. C. LOOI, *Composites* **26** (1995) 767.

Received 1 December 1994
and accepted 1 December 1995